power supply unit, electrocautery tip electrode, discharge target, and counter electrode plate. The amount of heat generated is expressed in equations (1) and (2).

$$W = I^2 R t_D \quad (1)$$

$$R = \rho \frac{l}{A} \quad (2)$$

Where W [J] is the amount of heat generated, I [A] is the effective current, R [Ω] is the electrical resistance of the biological tissue, and t_D [s] is the discharge time. The electrical resistance R of the biological tissue is calculated from the electrical resistivity of the tissue ρ [Ω/cm], the cross-sectional area of the current path A [cm^2], and the length l [cm]. To accurately control the discharge time t_D, a discharge control system was used to enable control of discharge and non-discharge in 1 ms increments. The discharge time is controlled by sending control commands from a personal computer to a microcomputer (Arduino Uno), which is then connected or disconnected via a relay device (G5NB 1A DC5V, Omron). The pencil type electrocautery that holds the tip electrode is attached to the electrocautery holder, and the position of the holder can be adjusted in 10 μm increments using a micrometer feed screw. This allows for adjustment of the electrode's insertion depth into the blood. The discharge target was set on a counter plate in a stainless steel container. In this experiment, the discharge times t_D was set to 1, 3, and 5 s, the power supply output P to 30 W, the power supply frequency f to 500 kHz, and the electrode insertion depth d to the discharge target to 2 mm.

The particle counting equipment was a light scattering particle counter (MET ONE HHPC 6+, Beckman Coulter). A light scattering particle counter was set 50 cm above the electrometallic discharge device in this experiment to count the number of particles per unit volume. The rated flow rate was 2.83 L/min, and the particle diameters measured were 0.5, 1.0, 2.0, and 5.0 μm. This is because particles with

a size of 0.5-5.0 μm are called lung damaging dust and reach the periphery of the lungs, causing acute and chronic inflammatory changes [2]. The measurement time was set to 30 s from the start of discharge. To eliminate the influence of particles in the experimental environment, the number of particles per unit volume in the experimental environment was measured three times before the discharge started. The smoke generation rate p was calculated by subtracting the average number of particles per unit volume in the environment from the number of particles $p_{measured}$ during discharge. Therefore, the amount of smoke generated is evaluated by the following equation (3).

$$p = p_{measured} - p_{environment} \quad (3)$$

Methods for measuring and analyzing electrical characteristics during discharge

An oscilloscope (TBS2072, Tektronix) was used to measure electrical characteristics during electrocautery discharge. In this experiment, the oscilloscope was connected to a voltage probe (P5002A, Tektronix) and a current probe (P6021A, Tektronix) on the circuit of the discharge device to measure the voltage and current during discharge. Since the power supply frequency was 500 kHz, the sampling frequency was set to 3.125 MHz based on the sampling theorem. Because the voltages and currents are alternating currents, the measurement results are discrete values that oscillate positively and negatively. Therefore, in this study, the practical values of the nth voltage and current, $f_e(n)$, were calculated using the nth measurement value, $f(n)$, and a constant number of measurement points, N, by the following equation (4):

$$f_e(t) = \sqrt{\frac{1}{N}\sum_{n-\frac{N}{2}}^{n+\frac{N}{2}} f(n)^2} \quad (4)$$

where N= 31,250 (0.01 s). The quotient of the voltage and current calculated from equation (4) was used as the electrical resistance value.

Method of measuring temperature distribution during discharge

During electrocautery discharge, an infrared high-speed camera (X6901sc, Photron) was used to measure the temperature distribution. In this experiment, a 1× magnification, 200 mm focal length objective lens was used to measure the temperature distribution of the liquid surface near the electrode insertion point during discharge by taking images from an angle of attack of approximately 45° to the liquid surface of the discharge target. The number of pixels captured was 640×512 pixels, the resolution of one pixel was 25 μm, the shooting speed was 300 fps, and the measurement temperature range was 35°C-350°C.
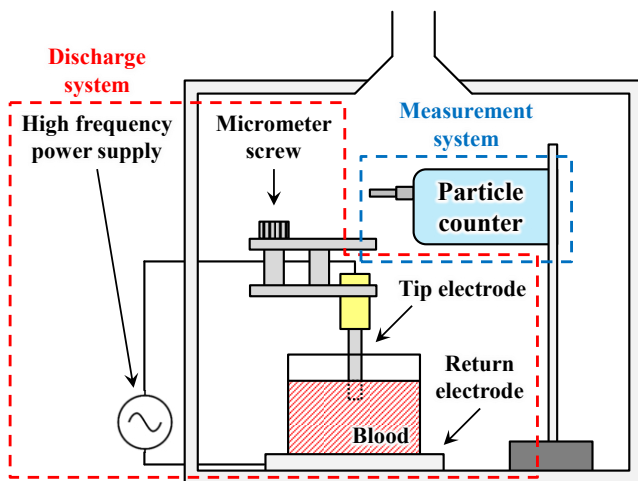

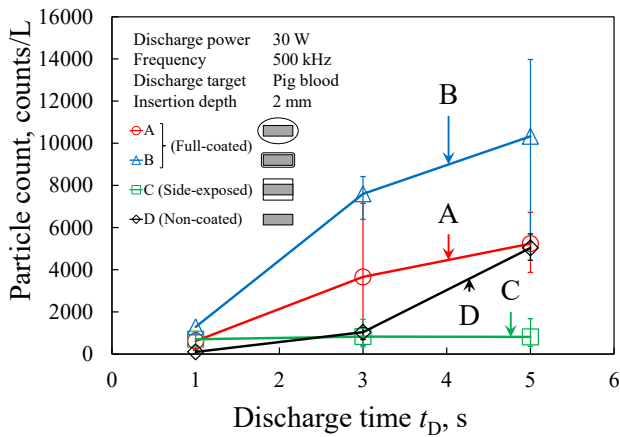**Figure 2:** Schematic diagram of the particle counting system

Figure 3: Total amount of smoke generated by each electrode

Results

Results of smoke generation measurements during discharge tests utilizing each electrode specimen

Figure 3 showed the measured smoke generation during discharge when discharge tests were conducted with coated electrodes A, B, and C and uncoated electrode D with discharge times t_D=1, 3, and 5 s. The number of particles per unit volume at t_D=1 s was approximately 618, 1286, 703, and 101 counts/L for each electrode, respectively. Electrode B showed the highest value, followed by electrodes A and C, with identical values. The particle counts at t_D= 3 s were approximately 3660, 7602, 829, and 1037 counts/L, respectively. The number of particles at electrodes A and B increased by approximately 5.9-fold compared to the case t_D= 1 s, with electrode B having the most significant value as in the case t_D= 1 s. The number of particles at electrode D increased approximately 10.2-fold compared to the case t_D=1 s. However, the number of particles at electrode C increased only approximately 1.2-fold compared to the case t_D= 1 s. Electrodes C and D had identical values. Moreover, the number of particles at electrode C increased only approximately1.2-fold compared to the case t_D= 1 s. Furthermore, the particle count at t_D= 5 s were approximately 5236, 10328, 812, and 5032 counts/L, respectively. The number of particles at electrodes A and B increased by 1.4-fold when compared to the case t_D= 3 s, with electrode B having the most significant value as in both t_D= 1 and 3 s. The number of particles at electrode D increased approximately 4.9-fold compared with the case t_D= 3 s and was comparable with the value at electrode A. The number of particles at electrode C remained constant, meaning it did not increase. Consequently, at t_D= 5 s, the number of particles at electrode C was 84%-92% lower than at the other electrodes. The results show that electrode C, whose side surface is not coated, has the most significant surgical smoke reduction impact.

Measurement results of electrical characteristics during discharge using each coated electrode specimen

Figure 4 shows the measured electrical resistance of coated electrodes A, B, and C and uncoated electrode D during discharge testing with a discharge time of t_D= 5 s.The electrical resistance of electrode A gradually increased soon after the initiation of the discharge and remained steady at approximately 940 Ω after t= 2.0 s. The electrical resistance of electrode B increased rapidly immediately after the start of discharge and continued to increase slowly until the end of discharge, reaching a maximum of approximately 2900 Ω. The electrical resistance of electrode C increased slowly soon after the initiation of the discharge and remained steady at approximately 920 Ω after t= 2.9 s.The electrical resistance of electrode D remained stable at approximately 150 Ω from the start of discharge until t= 1.0 s, after which it increased rapidly until t= 1.5 s and continued to increase slowly until the end of discharge, reaching a maximum value of approximately 2200 Ω.

Observation results during discharge using an infrared high-speed camera using each electrode specimen

The temperature distribution results observed by a high-speed infrared camera during discharge and specimen observation after discharge are shown in figure 5 (a) and (b), respectively. The discharge tests were conducted using an uncoated electrode D and a coated electrode C whose electrode side surface was not covered with a coating, with a discharge time t_D= 5 s. When electrode D was used, the heat was concentrated on the electrode's side surface immediately after the discharge started to t= 1.1 s. Then the heat was transferred from the side surface to the flat surface of the electrode from t= 1.4 s onward. Bubbles were observed near the electrode insertion point from t= 1.2 s to 2.8 s. Additionally, a severe arc-like heating phenomenon was detected at the entire electrode insertion point after t= 2.9 s.
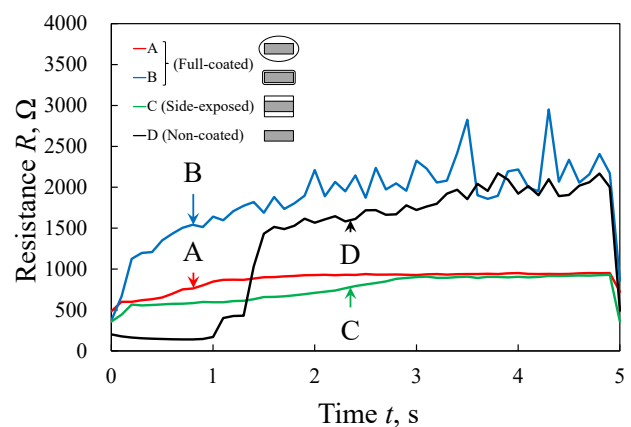

Figure 4: Time variation of electrical resistance of each electrode

The bubbles were observed to be generated by the electrode insertion point, as well as the electrode insertion area from $t =$ 2.9 s onward. The maximum temperature in the vicinity of the electrode insertion area increased gradually immediately after the discharge began, reaching approximately 120 ºC at $t= 1.3$ s and remaining stable at approximately 100°C until $t= 2.8$ s. When an arc-like heat-generating phenomenon was detected at the electrode insertion point, a maximum temperature peak of around 280°C was observed. Furthermore, the whole surface of the electrode was coated with coagulated blood after the discharge. When electrode C was utilized, however, heat was concentrated on the side surface of the electrode from the start of discharge to the end of discharge, and heat was observed to be transmitted from the side surface of the electrode to the flat surface of the electrode. Additionally, heat convection outward from the electrode's side face was observed after time $t= 2.0$ s. Furthermore, from the beginning to the completion of the discharge, the side surface of the electrode was hotter than the flat surface of the electrode. The maximum temperature around the electrode insertion area increased rapidly after discharge began, reaching approximately 90 ºC at $t= 0.9$ s and remaining stable at approximately 80 ºC until $t= 4.2$ s. Following the discharge, the uncoated side surface of the electrode and the electrode tip were found to be sparsely coated with coagulated blood.
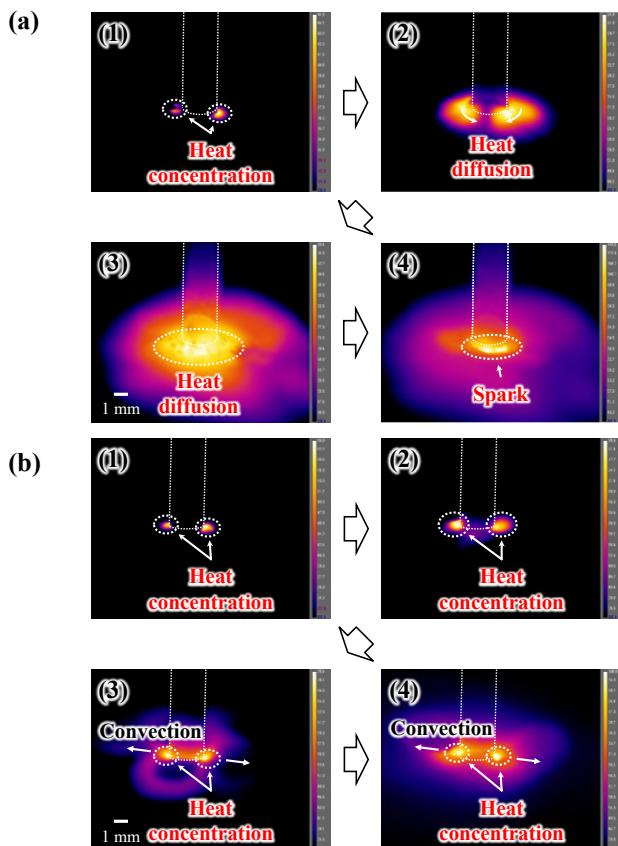

Figure 5: (a) Results of infrared high-speed camera observation of electrode D and **(b)** electrode C
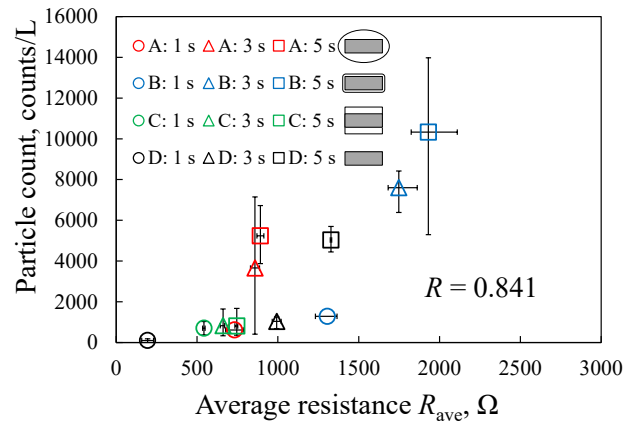

Figure 6: Relationship between average electrical resistance and surgical smoke generation for each experimental condition

Discussion

Effect of electrical resistance during discharge on the amount of smoke generated

The side surface of the electrode was not coated after the discharge, where as the tip of the electrode was sparsely coated with coagulated blood. The influence of electrical resistance during discharge on the amount of smoke generated during discharge experiments utilizing coated electrodes A, B, and C and uncoated electrode D is discussed based on the experimental results. Figure 6 shows the average electrical resistance under each experimental setting. Both metrics showed a strong positive relationship with a correlation coefficient of $R= 0.841$. This implies that the increase in electrical resistance during discharge has a significant influence on the amount of smoke generated and that the amount of smoke generated can be minimized by suppressing the increase in electrical resistance during discharge.

Effect of coating geometry on electrical properties and smoke generation during discharge

Based on the experimental results, the influence of the coating shape on the electrical resistance during discharge is discussed when discharge tests are conducted using coated electrode C, whose electrode side surface is not covered with a coating, and uncoated electrode D. Figure 7 shows a schematic diagram of the electrical resistance rising model and an electrical circuit model when discharge experiments with electrodes C and D were conducted. In the case of electrode D, the temperature distribution observation results shown in figure 5 confirm that heat was transferred from the electrode's side surface to the electrode's flat surface, and bubbles were generated from the electrode insertion area. It was also confirmed that intense arc discharges occurred over the entire electrode insertion area after the middle stage of the discharge. This suggests that the transition from a boiling state to film boiling caused the formation of a vapor film
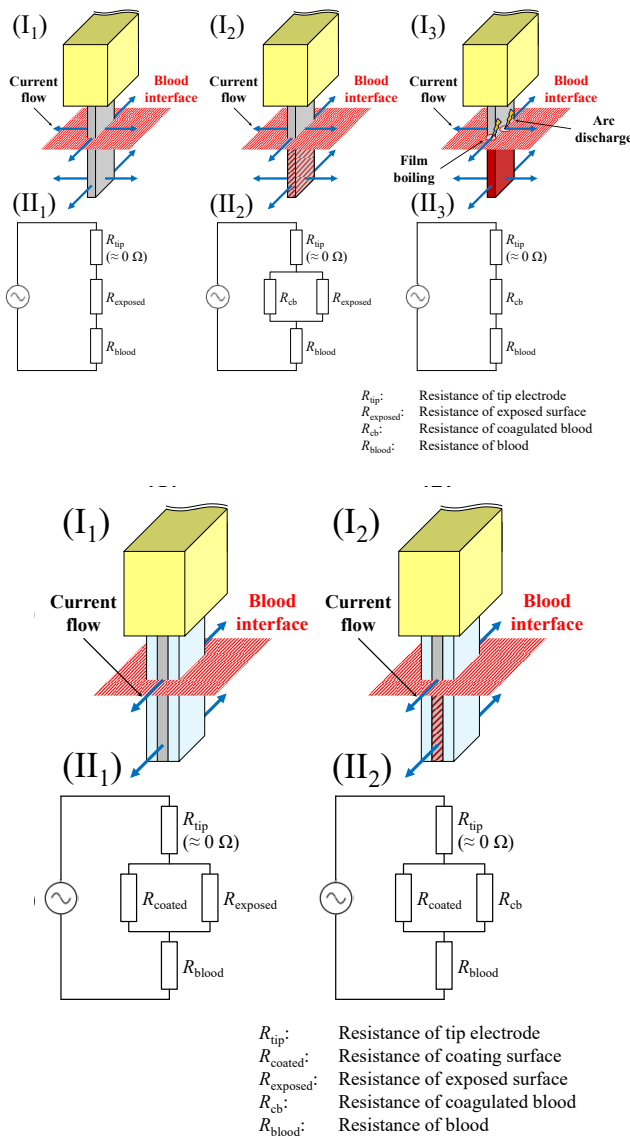
Figure 7: (a) Electrical resistance schematic diagram and circuit model of electrode D and **(b)** electrode C

the coating, and the tip of the electrode, were slightly coated with coagulated blood. The exposed metal surface of the electrode's side face enhanced thermal convection, causing bubbles to detach from the electrode insertion area and preventing the transition to film boiling. This is considered to have suppressed the transition to film boiling, preventing an increase in Joule heat and the generation of arc discharge, and therefore reducing the amount of smoke generated.

Conclusions

In this study, to investigate the feasibility of an electrocautery surface coating that suppresses surgical smoke, we evaluated the amount of smoke generated by discharge tests using an electrocautery tip electrode with a coating of different cross-sectional shapes and an uncoated electrode and proposed a model of increased electrical resistance due to coagulated blood adhesion in an electrical circuit model that included the electrode, silicone coating, and discharge target. The effect of increasing electrical resistance increase on the amount of smoke generated was evaluated. The method by which the electrocautery surface coating affects smoke generation was explored using a high-speed infrared camera to measure the temperature change in the region of the electrode during the discharge. The following are the significant results obtained.

(1) Discharge tests were conducted utilizing coated electrodes A, B, and C and uncoated electrode D with varied coating geometries, and the amount of smoke generated during discharge was evaluated by measuring the number of particles per unit volume. The particle counts for coated electrodes A and B and uncoated electrode D at discharge time t_D = 5 s were approximately 5236, 10328, 812, and 5032 counts/L, respectively. Nonetheless, the number of particles on coated electrode C, whose side surface was not coated, was 812 counts/L, which is approximately 92% lower than the number of particles of other electrodes. This indicates that electrode C has the most significant smoke reduction effect.

(2) Discharge tests were conducted, and the electrical resistance during discharge was determined. Coated electrodes A and B and uncoated electrodes D's electrical resistance were 940, 2900, and 2200 Ω, respectively. However, the electrical resistance of coated electrode C reached approximately 940 Ω. The increase in electrical resistance was suppressed compared with other electrodes. A significant positive correlation coefficient R = 0.841 was obtained between the average electrical resistance and the amount of smoke generated under each experimental condition. This indicates that the electrical resistance during discharge has a significant impact on the amount of smoke emitted. Therefore, it was established that the amount of smoke generation could be reduced by suppressing the increase in electrical resistance during discharge.

on the electrode surface, which became an insulating layer, resulting in the generation of arc discharges. Furthermore, the postdischarge observation results confirmed that coagulated blood coated the whole surface of the electrode. This implies that the coagulated blood attached to the flat surface of the electrode from the side surface and formed an electrical resistance layer, increasing electrical resistance and Joule heat. The afore mentioned reasons have increased the amount of smoke generated. In the case of electrode C, the temperature distribution observation results shown in figure 5 confirm that heat convection flowed outward from the side surface of the electrode during the discharge. The postdischarge observation results confirmed that the side surface of the electrode during the discharge. The postdischarge observation results confirmed that the side surface of the electrode, which is not covered by

Citation: Takayuki Tokoroyama, Motoyuki Murashima, Koki Ogawa, Noritsugu Umehara, Hosei Nagano, Takayuki Yorozu, Junichi Uchida. Development of an Electrocautery Surface Coating Method to Suppress Surgical Smoke. Journal of Surgery and Research. 7 (2024): 53-59.

(3) The mechanism of smoke reduction at the coated electrode was examined by observing the temperature distribution using a high-speed infrared camera during discharge. When electrode C was used, outward heat convection was detected from the side surface of the electrode during discharge. This is probably due to the concentration of current and heat on the electrode's side face of the electrode's metal surface of the side face of the electrode was exposed, which increases the current density. This suppressed the transition of the boiling state to film boiling and the growth of coagulated blood and suppressed the increase in electrical resistance, which lowered the amount of smoke generated.

Disclosure

Approval of the research protocol: N/A

Informed Consent: N/A

Registry and Registration No. of the study/Trial: N/A

Animal Studies: N/A

Conflict of interest: The authors declare no conflicts of interest associated with this manuscript.

References

1. Tokoroyama T, Kobayashi M, Murashima M, et al. Preventing coagulated-blood adhesion on a coated electrosurgical knife. Transactions of the JSME 86 (2020): 20-00273.

2. Alp E, Bijl D, Bleichrodt RP, Hansson B, Voss A. Surgical smoke and infection control. J. Hosp. Infect 62 (2006): 1-5.

3. Ulmer BC. Air Quality in the Operating Room. Surg. Serv. Manag 3 (1997): 14-16.

4. Ulmer BC. The Hazards of Surgical Smoke. AORN J 87 (2008): 721-734.

5. Barrett WL, Garber SM. Surgical smoke: a review of the literature. Surg. Endosc 17 (2003): 979-987.

6. Fitzgerald JEF, Malik M, Ahmed I. A single-blind controlled study of electrocautery and ultrasonic scalpel smoke plumes in laparoscopic surgery. Surg. Endosc 26 (2012): 337-342.

7. Chadi SA, Guidolin K, Caycedo-Marulanda A, et al. Current Evidence for Minimally Invasive Surgery During the COVID-19 Pandemic and Risk Mitigation Strategies. Ann. Surg 272 (2020): e118-e124.

8. George R, Robert U, Rami I, Han TW. Minimizing the Risk of Aerosol Contamination During Elective Lung Resection Surgery. Ann. Surg 272 (2020): e125-e128.